Asymmetric electrode-molecule transport dynamics tracked by nanoscale electroluminescence

Jose I. Gonzalez, Tom Vosch, and Robert M. Dickson*
School of Chemistry and Biochemistry and Petit Institute for Bioengineering and Bioscience, Georgia Institute of Technology, Atlanta, Georgia 30332-0400, USA

(Received 17 February 2006; revised manuscript received 3 April 2006; published 16 August 2006)

Common to molecular electronics studies, nanoscale break junctions created through electromigration naturally produce electroluminescent arrays of individual gold nanoclusters spanning the electrodes. The arrival time stamping of detected photons from these electrically driven, room-temperature nanoclusters demonstrates that charge injection to the clusters is directly modulated by dynamic coupling to individual electrodes. These several-atom nanoclusters electroluminesce due to inelastic electron tunneling into cluster electronic energy levels. ac electrical excitation (~200 MHz) with time-stamping of photon arrival times enables fast and local tracking of electrode-nanocluster coupling dynamics. The electrode-nanocluster coupling rate fluctuates by nearly an order of magnitude, and due to the asymmetry of the electromigration process, exhibits preferential charge injection from the anode. Directly reporting on nanoscale charge transport, time-tagged single-molecule electroluminescence reveals a significant mechanism for nanoscale charge transport in nanoscale gold break junctions and offers a direct readout of the electrode-molecule interactions that can be correlated with current flow.

DOI: 10.1103/PhysRevB.74.064305 PACS number(s): 78.60.Fi, 78.67.Bf, 85.60.Jb

I. INTRODUCTION

While crucial to the understanding of nanoscale transport physics, the nonequilibrium dynamics of electrode-molecule coupling by an external electric field are not well characterized and become washed out in conventional time-averaged molecular electronics experiments.[1–6] As even state-of-the-art nanofabricated electrodes[7,8] are much larger than molecular dimensions, many conduction pathways and mechanisms of charge transport through and around the molecule are active, further obscuring interpretations. While bulk conduction through an insulating layer typically occurs via capacitive charge-discharge cycles or short-range tunneling, charging effects on the nanoscale become quantized and tunneling dominates through available resonant channels.[9,10] Routinely demonstrated in the absence of high-efficiency resonant pathways,[4,6,9,11–13] quantized charging and coulomb blockade are exhibited at temperatures for which available thermal energy is smaller than the energy level spacings of a bridging nanoparticle.

When an external field is strong enough to overcome the deep confinement potential posed by the metal-insulator interface, nonresonant tunneling (field emission) ensues and decreases exponentially with interelectrode distance.[14] Introduction of a molecule into the junction mediates tunneling of electrons resonant with its discrete energy levels by providing a nonzero charge density within the barrier potential.[8] Depending on the strength of coupling to each electrode, molecule-mediated tunneling processes can also proceed inelastically as the injected electrons lose energy to transitions between vibrational or electronic states. Nearly 40 years ago, Lambe and co-workers reported peaks in the differential conductance of molecule-doped metal-insulator-metal junctions.[15] The peaks, appearing at a few tens of millielectronvolts, were both IR- and Raman-active vibrational modes of the dopant molecules resulting from inelastic tunneling. More sophisticated versions of these experiments have been carried out on the single molecule scale within three-terminal devices[6,16–18] and scanning tunneling microscopes.[19–21] Electrically driven mechanical vibrations of fullerenes[6,16] and optical transitions of individual noble metal nanoclusters[22,23] and semiconductor quantum dots[17,18] were also recently reported. Such inelastic tunneling through electronic transitions was predicted[24] in 1968, and electroluminescence (EL) was observed soon thereafter.[25,26]

Recently, we have studied electroluminescent metal-insulator-metal junctions to probe optoelectronic dynamics of individual small gold,[22,23] silver,[27,28] and copper[29] molecular-scale clusters. While nanocluster emission is highly dependent on the material, all cluster systems exhibit bright EL under both dc and ac electric fields. Important both as electrodes in nanoscale electronics[6–8,13,16,30] and as size-tunable quantum dots,[31] nanoscale gold has many promising optoelectronic properties. Even many-body electron spin correlations attributed to small gold clusters have been observed[30] in recent low-temperature electrical measurements of nanoscale gold break junctions. Because we can track the electrode-nanocluster coupling dynamics by counting EL photons, single molecule electroluminescence constitutes the first corroborative and noncontroversial readout of nanoscale current flow. While an inefficient charge-transport pathway, inelastic electron tunneling through radiative electronic states provides a noninvasive probe of nanoscale junction dynamics. With high-frequency ac excitation such that charge injection and excited state lifetimes are comparable to the excitation period, time-tagged electroluminescence photon counting provides previously inaccessible, background-free information about the field and injection dynamics within nanoscale break junctions.

II. MATERIALS AND TECHNIQUE

To create electroluminescent junctions, we thermally evaporate 20 nm thick gold films on glass substrates. Sub-

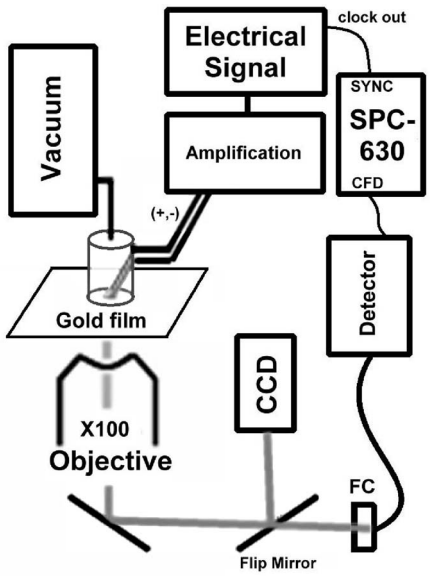

FIG. 1. Time-tagged, time-correlated, single-photon counting setup for measurement and imaging of gold nanodot electroluminescence. An electrical waveform generator and amplifier excites the gold electromigration-induced break junction held under vacuum (10^{-5} Torr) by an oil-free turbopump (Varian). The electroluminescence is collected through a 1.4 NA, 100× microscope objective and either imaged on a CCD or focused through an optical fiber and passed to a Perkin Elmer avalanche photodiode. The detector signal is passed to the CFD (start) of a Becker & Hickl SPC-630 photon counting module and synchronized by either the frequency-divided excitation clock (Pulse Research Lab, PRL-260NT) or an external clock (stop).

strates are transparent and thin enough to enable imaging with a 1.4 numerical aperture (NA) oil-immersion objective mounted on an optical microscope (Fig. 1). Two leads are attached to the gold surface and the entire assembly is placed under vacuum as previously described.[22] The sample holder and electrode assembly are encased with mu-metal to prevent rf interference with other instruments. Under dc bias, momentum transfer from electrons to the Au atoms results in void formation at some critical current density and temperature combination.[32] Film resistance rises dramatically as this void enlarges to break the film. Commonly known as electromigration, this phenomenon is often employed to produce very small break junctions in metal wires.[7] In the presence of a constant dc potential at or above some critical level (~2.5 V), the junction formation can be monitored by measuring increasing film impedance. The final junction impedance reaches $>10^6\ \Omega$ in a few seconds, with a total charge consumption on the order of 1 $C/\mu m^2$. Since the fabrication process is carried out under constant polarity, the mechanical forces generated by the external field serve to structurally and chemically polarize the metal film. As a result, slight structural asymmetry is incorporated into the junction and is observable by both optical and electrical measurements that differ between Au and Ag due to the different electromigration conditions and chemical reactivities with respect to oxidation. The final junction is very heterogeneous with many subnanometer interelectrode gaps. Dramatic irreversible changes in film morphology after electromigration-induced breaking also allow monitoring of junction formation by observing film optical properties. This asymmetric change in the film refractive index makes the junction easily discernible by phase contrast microscopy [Fig. 2(b)], suggesting the creation of a heterojunction as opposed to the homojunction behavior commonly assumed when utilizing such gold break junctions for molecular electronics studies.[4–7,33]

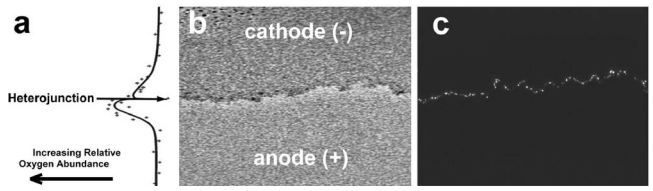

FIG. 2. (a) Energy-dispersive spectroscopy of a typical gold film after electromigration-induced junction formation showing relative oxygen content (horizontal axis) vs distance from the junction (vertical axis). Each point represents integration over a 1 μm square. The line through the data is only a guide for the eye. (b) Optical phase contrast micrograph of the gold junction in (a) collected immediately after electromigration. (c) Electroluminescence image collected through a 1.4 NA objective using a CCD (Micromax, Princeton Instruments). A ±2.5 V ac signal at 205 MHz was used as the electrical excitation.

Spatially-resolved electron energy dispersive spectroscopy (EDS) probes electrode chemical composition [Fig. 2(a)], revealing slightly higher oxygen content on the anode. During junction formation, gold undergoes an asymmetric combination of thermal and electrochemical oxidation, consistent with our observed chemical composition. The final result is a disordered array of isolated gold nanodots created within the break junction in a gold-insulator-Au_n-insulator-gold configuration. Electrochemical and x-ray photoelectron spectroscopic studies[34,35] of oxide formation on gold surfaces suggest that the atomic configuration of these oxide regions may be a mixture of insulating auric oxide (Au_2O_3) and gold hydroxide [$Au(OH)_3$] created from physisorbed water and hydroxyl moieties. These oxygen-rich insulating layers are analogous to the aluminum oxide tunneling barriers employed in conventional inelastic electron tunneling spectroscopy (IETS) measurements.[24] Large band-gap insulators such as Al_2O_3 are an indispensable element of these systems because they electrically isolate the leads from the analyte being studied. Separation of the gold nanodots from metallic electrodes enables charge transport through clusters while preserving their low density of states near the highest occupied molecular orbital-lowest unoccupied molecular orbital (HOMO-LUMO) gap. Without the insulating gap, the metallic electrodes' continuous density of states would broaden the molecule's discrete states, precluding sharp tunneling resonances, charge separation, or observable electroluminescence.[36] As we now report, under continued electrical excitation, bright near-IR electroluminescence is observed from gold clusters, providing a map of the junction [Fig. 2(c)] which is otherwise too narrow to characterize by optical methods. While only small, several-atom clusters with discrete states electroluminesce, typical electromigrated

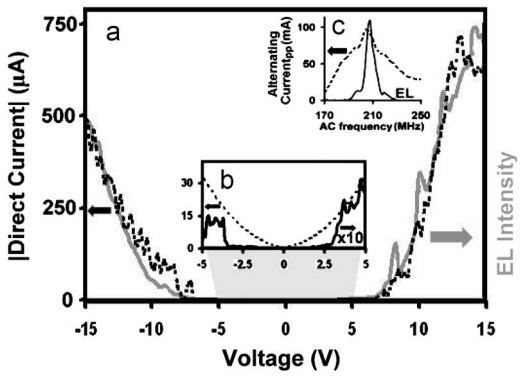

FIG. 3. Time-averaged electrical (dotted traces) and optical (solid traces) response of a gold junction after electromigration. (a) Comparison of the typical electrical and optical response of the junction with peaks arising from stochastic events transiently altering emission intensity. Peaks above 5 V are not reproducible between successive scans. The noise floor of the ammeter used here (Agilent E3646A) is approximately 100 μA and has been subtracted from the data. (b) Low-voltage dc measurements of the junction current (dotted), using a Keithley 6485 picoammeter, and EL intensity (solid). (c) Frequency response of the total junction current (dotted) and EL (solid). AC current amplitude was measured using an rf transformer (Solar Electronics 9203-1) placed around the cathode.

gold junctions are very heterogeneous and may contain much larger isolated grains.[13]

III. RESULTS AND DISCUSSION

For applied biases of more than 3 V dc, light emission is observed from individual gold nanoclusters, and electroluminescence intensity increases with increased current flow [Fig. 3(a)]. Transport through room-temperature gold break junctions is monitored by observing the electroluminescence from individual several-atom gold clusters and overall current through the whole junction. Emitted light is either routed (Fig. 1) to a charge-coupled device (CCD) camera for imaging or spatially filtered by fiber coupling to an avalanche photodiode (APD). Electrical pulses from the APD are properly conditioned and counted by a Becker & Hickl photon counting module.[37,38] As electrons pass through the insulating gap, they inelastically tunnel through both vibrational and vibronic levels of junction-bound gold molecules which act as temporary charge reservoirs. Initial hole injection (ionization) followed by electron injection results in recombination, yielding electroluminescence.[22] Above ~10 V dc, gold nanodots within the junction are thermally or oxidatively destroyed. Consequently, the cavity conductance and electroluminescence irreversibly increase with voltage to produce the peaks observed in the current and emission intensity [Fig. 3(a)]. The electrical and luminescent properties of the junction under low-voltage dc excitation [Fig. 3(b)] are typically stable for a few hours of continuous operation, and EL has been observed at biases as low as +2.5 V dc.

Similar gold electrodes fabricated using electromigration-induced break junction techniques[7,13,30] produce many interelectrode spacings measuring <10 nm. Purely electrical characterization of these systems is limited by inherent averaging over the entire cross-sectional area of the junction. Therefore, proper characterization of the electrodes in single molecular devices ultimately requires a single-molecule probe of the local electric field and electrode-molecule coupling, both before and after introducing the molecular bridge. Because light emission from gold nanoclusters is representative of the applied potential and the coupling to individual clusters, electroluminescence provides a local measurement of the electric field within the junction with higher sensitivity than possible with electrical measurements. Simultaneously measurable with current flow, nanoscale EL avoids contributions to the current from other conducting pathways and charge-transport mechanisms, thereby providing corroborative and complementary information on local transport dynamics.

As electromigration is a destructive process, even the initially formed gold electrodes will further restructure under constant dc bias. Below a certain current level, dc electromigration-induced junction restructuring is minimal and the electrodes adopt a stable structure. Applying a larger dc bias across the electrodes restructures them further to a new morphology stable at the new voltage level. At 5 V bias, the total current through a typical ~100 μm junction [Fig. 4(a)] decreases steadily for the first 500 s, from an initial value of 35 μA to 23 μA. A period of large, repeated current fluctuations follows from 500 s to 1200 s as the junction stabilizes. After 1200 s at constant 5 V bias, the current fluctuations never rise above 2 μA, suggesting that junction reorganization is minimal. After 1200 s, the slow decrease in the current (<1 μA over 1 h) corresponds to the junction's gradual irreversible destruction brought about by heat and additional electromigration of the relatively high voltage dc field.

To minimize restructuring and stabilize emission, the junction-forming dc bias can be immediately switched off in favor of lower voltage, impedance-matched (ac) EL excitation. Matching the junction's natural resonance frequency produces strongly enhanced EL observed under high-frequency ac excitation [Fig. 3(c)]. At the junction resonance frequency (typically between 190 and 240 MHz), capacitive and inductive reactances exactly cancel, resulting in a true resistance of ~50 Ω for the circuit. This resonance exclusively results from the junction electrical properties (series RLC circuit), and correlates with the electroluminescence due to increased charge flow. The resonant ac operating conditions produce strong EL and greatly increased stability at lower voltage than does the more thermally destructive dc excitation. At the junction resonance, ac current through the junction reaches ±50 mA [Fig. 4(d)] with peak-to-peak current fluctuations no greater than 100 μA for the duration of the experiment. Spatially resolved electroluminescent features result from individual gold nanocluster emission as evidenced by blinking, dipolar emission patterns and antibunched EL.[22] Based on the jellium free-electron model and previous solution studies of gold nanodots,[31] Au nanocluster transition energies (~1.8 eV) scale with inverse cluster radius, suggesting that these transition energies result from ~18 to 22 atom gold particles.[22]

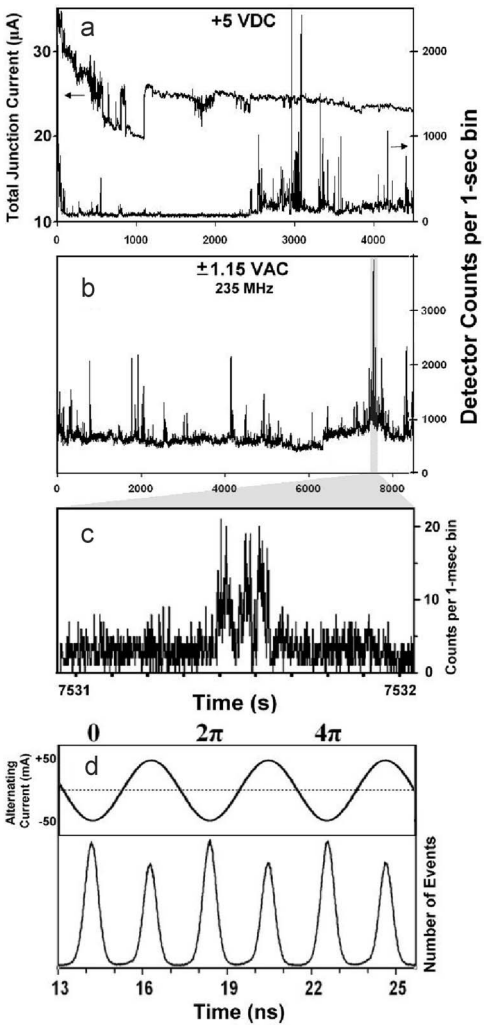

FIG. 4. Time traces of electroluminescence intensity and total junction current under (a) dc and (b,d) ac bias. Electroluminescence was measured in the configuration shown in Fig. 1. The dark count rate of our Perkin Elmer avalanche photodiode is approximately 100 Hz. DC and ac current were measured as in Figs. 3(b) and 3(c), respectively. (a) A 4500 s series of total junction current measurements (300 ms bins) and EL intensity detected from an individual cluster under a constant +5 V dc field. (b) An 8500 s time series of EL intensity detected from an individual gold cluster in ±1.15 Vac external field at 235 MHz. EL time series in (a) and (b) are binned by 1 s. The sudden shift in EL intensity in (b) at ~6100 s is an artifact of refocusing the image to correct for mechanical drift of the optics. (c) EL time series in (b) rebinned by 1 ms in the range 7531–7532 s. (d) AC mode electroluminescence decay trace (histogram) collected by phase-locking to the excitation field. Three periods of the excitation are shown for all photons collected over the entire 8500 s interval; the EL decay trace bin width is approximately 12 ps.

Typical dc mode electroluminescence [Fig. 4(a)] excited at +5 V results in periods of intense light emission separated by long, dark periods in which no EL photons are detected. In contrast, typical ac mode electroluminescence [Fig. 4(b)] rarely turns off for periods longer than 1 s, as demonstrated by the baseline EL count rate of approximately 600 Hz. Frequent bursts of electroluminescence intensity rise above this baseline to reach detected count rates as high as 4 kHz. The fast intensity fluctuations observed in Fig. 4(b) can be further resolved by 1 ms binning, and expansion of the 4 kHz spike at 7531 s [Fig. 4(c)] reveals a series of much shorter bursts (<10 ms duration) in rapid succession, reaching more than 20 counts per 1 ms bin. It is interesting to note that while ac excitation is applied at lower voltage than is the dc field, the resonant ac mode produces more photons per second and higher peak intensities during bursts. This discrepancy likely arises from clusters only needing to couple to one electrode for ac EL. Since charge must flow *through* the junction in dc excitation and *around* the junction in ac excitation, efficient dc EL requires weak but significant nanocluster coupling to both electrodes, while ac EL requires such coupling to only one. These coupling rules suggest that a given nanocluster is more likely to electroluminesce in an ac field than in a dc field of equivalent voltage. Because each ac-driven photon corresponds to hole and electron injection from the same electrode,[22] and injection from the electrodes is separated in time by the oscillating field polarity, all information about the anode- and cathode-nanocluster coupling dynamics contained in the ac EL time series is separable.

An on-board 20 MHz macrotiming clock (Becker & Hickl SPC-630) provides the timing resolution to build the chronological EL-photon arrival time series shown in Figs. 4(a)–4(c), with bin widths down to 50 ns. In all experiments, the APD counts routed to the constant fraction discriminator (CFD) are further referenced to an external clock. In the case of dc mode electroluminescence, an external pulse generator stops the time-to-amplitude conversion in the photon counting module. Because such an external pulser is not synchronized with the EL excitation, no dc EL decay information is collected. However, modulation of the excitation field as in ac mode enables phase-locked synchronization of the CFD to the EL excitation, analogous to the synchronization of a fluorescence signal by a modulated laser in a frequency-domain lifetime measurement. ac mode EL photon arrival times are thus synchronized to the same ac excitation field that drives the electroluminescence, and it is possible to gather phase information from each EL photon. Electronically dividing the excitation clock frequency by an integer, N, (Pulse Research Lab, PRL-260NT) allows phase-locked detection of EL pumped above the 200 MHz synchronization limit of our Becker & Hickl SPC-630 time-to-amplitude converter while producing histograms spanning N complete excitation periods. Using this phase information, we can build a histogram of the EL decay profile [Fig. 4(d)]. The histogram shows two EL peaks for every full period (2π) of the excitation sine wave. For the 235 MHz excitation field applied, the full 13 ns window shown here contains six peaks and three complete periods (6π). In each period, the first peak at 0 corresponds to EL resulting from charge injection through the anode and is more intense than the second peak appearing near π.[22] The smaller peak near π corresponds to gold nanodot EL resulting from cathode injection. Because the potential applied across the junction is an oscillating field of alternating polarity, the electric field driving charge injection from the anode side is identical to that from the cathode side but shifted in phase by π. The intensity difference between anode and cathode peaks is then a direct result of asymmetric

coupling between the electroluminescent gold cluster and the electrodes used to inject charge. Any electrode chemical asymmetry (Fig. 2) only minimally affects the charge injection asymmetry. The original junction polarization resulting from electromigration likely plays a major role. As a compilation of all photons in the 8500 s time series, the histogram [Fig. 4(d)] represents a time-averaged picture of the electroluminescent junction asymmetry, revealing a slight preference for nanodot charge injection from the anode over that from the cathode. It is interesting to note the narrow linewidth of the peaks in the histogram as compared with the broader sinusoidal (±1.15 V ac) excitation field used to generate them. This narrowing is a direct result of the discrete nanocluster energy levels and inelastic electron tunneling into these states. As the same two-pulse polarity is observed for Au EL as that reported previously for Ag,[28] a hole must first tunnel from the injecting electrode into the bridging nanocluster's ground state and an electron must follow, one-half period later, tunneling into a discrete cluster excited state. Confirmed by extensive pulse-excitation data (in preparation), this process results in characteristic cluster turn-on voltages, as evidenced by narrow EL excitation peaks. Consistent with previously reported EL lifetimes of ~400 ps and our 500-ps-limited detection, the peaks in the histogram appear largely symmetric, with a small observable exponential component from the subnanosecond cluster radiative decay.

In both ac and dc mode operation, the applied electric field raises the chemical potential of one electrode with respect to the other as it drives the system away from equilibrium. These conditions give rise to time-dependent charge transport through the junction. Comparison of the relative peak heights in the EL decay histogram indicate that for long times, the relative coupling strengths between cluster and electrode slightly favor anode injection. By synchronizing detection to the oscillator driving the ac mode EL, we ensure that the photon arrival times contain phase information corresponding to the excitation field. It is then possible to separate out the different electrode contributions to the chronological EL time series by analyzing (or postacquisition gating) it in different phase ranges. The EL time series containing only photons within the range $(-\pi/2, \pi/2)$ provides time-dependent information about the anode-cluster coupling strength.[22] Similarly, the EL time series of only photons within the range $(\pi/2, 3\pi/2)$ provides time-dependent information about the cathode-cluster coupling strength. Within any microtime histogram, the normalized difference of these two contributions to the EL time series is given by

$$A(t) = \frac{EL_{-(\pi/2),(\pi/2)}(t) - EL_{(\pi/2),(3\pi/2)}(t)}{EL_{-(\pi/2),(\pi/2)}(t) + EL_{(\pi/2),(3\pi/2)}(t)},$$

and represents the time-dependent charge injection anisotropy for a specified binning time. When $\boldsymbol{A}(t) > 0$, charge transport through the cluster resulting in electroluminescence is dominated by injection from the anode. Times for which $\boldsymbol{A}(t) < 0$ correspond to EL from cathode injection. When $\boldsymbol{A}(t) = 0$, the electroluminescent cluster is coupled equally to both electrodes.

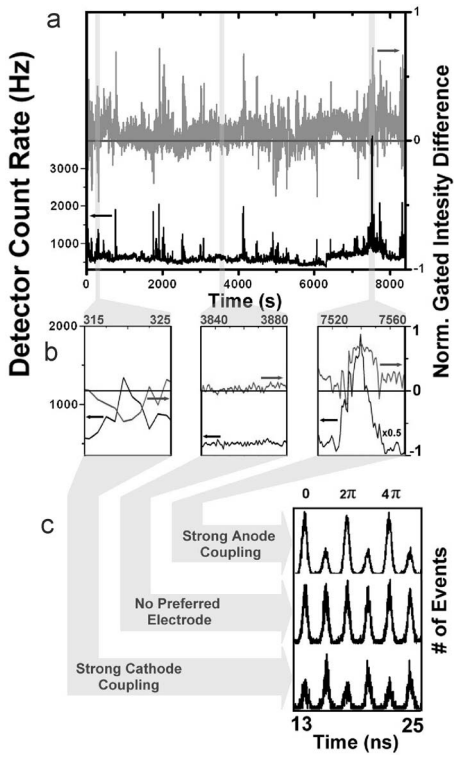

FIG. 5. Normalized gated EL intensity difference (gray) alongside the total ac mode EL intensity (black). (a) The full 8500 s time series is expanded for ease of viewing (b) at the three regions denoted by vertical gray bars. (c) EL decay traces corresponding to each expanded region of the time series showing three distinct electrode coupling regimes. Three periods of the excitation are shown.

A plot of the normalized gated intensity difference, $\boldsymbol{A}(t)$, is shown in red [Fig. 5(a)] alongside the total EL time series shown in black. As expected from the time-averaged EL decay histogram [Fig. 4(d)], junction transport shows an overall preference for anode injection with $\boldsymbol{A}(t) > 0$ for most of the time series. The mean value of $\boldsymbol{A}$ for the entire 1 s binned time series is +0.080 with minimum and maximum values of −0.48 and +0.71, respectively. It is interesting to note that large changes in the gated intensity difference occur in short bursts with similar duration as the bursts in EL intensity. In fact, side by side comparison of the intensity and gated intensity difference reveals a high degree of correlation. The coincidence of peaks in the two traces indicates that the electroluminescence bursts in the total intensity time series [Fig. 4(b)] are a direct result of large-amplitude, short-lived changes in the cluster electrode coupling strength. As mentioned above, the arithmetic sign of the bursts in the red trace indicates the electrode to which the coupling has increased. The time required to transition from equal coupling to either strong anode $[\boldsymbol{A}(t) > 0]$ or cathode $[\boldsymbol{A}(t) < 0]$ coupling is typically <10 ms. Times at which the gated intensity difference is low (slightly different from 0) correspond to the weak constant "on" state with an electroluminescence rate of ~600 Hz, suggesting that at these low voltages, the cluster rarely couples strongly to both electrodes at once. An estimate of the junction's injection efficiency, obtained by correlating EL emission rate with excitation rate,[39] indicates in-

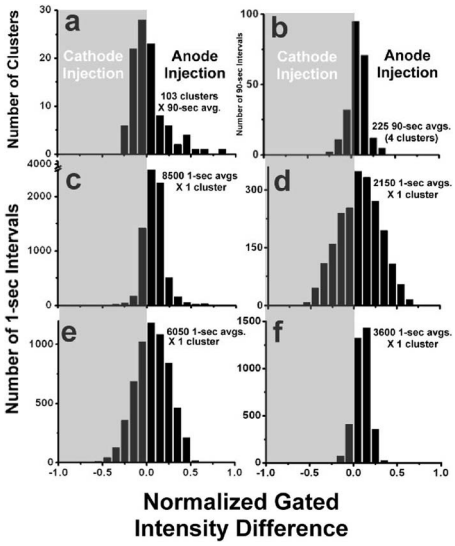

FIG. 6. Histograms of the normalized gated intensity difference, $A(t)$, for 103 gold nanoclusters. (a) The 90 s averaged $A(t)$ value for 103 individual clusters is provided for comparison with (b) the 90 s averaged $A(t)$ value sampled 225 times from four representative gold nanoclusters summarized individually in (c) through (f), each with 1 s binning.

jection rates of 22 MHz and 3.3 MHz for the "strong" and "weak" coupling regimes, respectively. Occurring on time scales much slower than the modulation frequency of the driving ac field, these large coupling rate fluctuations are likely also present under dc fields. The coupling fluctuations are still fast enough to be obscured by time-averaged dc transport measurements and may give rise to large variances in perceived junction dc conductance. The time-dependence of transport tracked by nanoscale EL illustrates the importance and need of additional dynamics studies in molecular electronics.

The observed cluster emission dynamics indicates three distinct coupling regimes which result in ac electroluminescence, namely, strong anode coupling, strong cathode coupling, and weak coupling to both. An example of each coupling regime is presented [Fig. 5(b)] by expanding portions of the full time series, denoted by vertical gray bars [Fig. 5(a)]. From left to right, the panels illustrate strong cathode coupling $[A(t)<0$, gray] with strong emission (black), no electrode preference $[A(t)\sim 0]$ with weak emission, and strong anode coupling $[A(t)>0]$ with strong emission. EL decay histograms containing only the photons in each expanded region are shown [Fig. 5(c)] for comparison with the full time series histogram [Fig. 4(d)]. The relative anode (2π) and cathode (π) peak heights are quite different for the strong coupling cases, while the middle histogram corresponding to the weak coupling regime shows identical peaks spaced by π.

The obscuring effect of averaging in nanoscale transport is also evident in the cluster injection anisotropy distributions. EL from a total of 103 nanoclusters was measured in the same way as above, but for shorter overall times. A histogram of the 90-s-binned A for the ensemble [Fig. 6(a)] has a mean value of +0.030 with a minimum of −0.29 and a maximum of +0.87, matching closely the dynamic range exhibited by the cluster in Fig. 5. Histograms of the 1-s-binned A for this cluster [Fig. 6(c)] and three other arbitrarily chosen clusters [Figs. 6(d)–6(f)], each observed for several hours as in Fig. 4, are shown for comparison. While the maxima, minima, and widths of each cluster anisotropy distribution vary, all histograms are asymmetric with a positive mean showing anode preference. Addition of the individual cluster histograms (c–f) and rebinning at 90 s results in a distribution of A sampled 225 times from four clusters [Fig. 6(b)]. For very high values of A, the tail in the ensemble-averaged distribution [Fig. 6(a)] is not yet observed in the subensemble time-averaged distribution [Fig. 6(b)]. This may be due to a combination of our limited observation times (a few hours per cluster) compared with our relatively large ensembles, and the greater environmental sampling inherent in averaging over many clusters between heterogeneous electrodes. Moreover, while the A value for transport through an individual cluster may vary dramatically, yielding a broad distribution [Figs. 6(d) and 6(e)], the distribution variance is significantly diminished when integrating for long times, as in (b), or over many transport pathways, as in (a). The qualitative similarities in anode preference and variance between the cluster-averaged A distribution (a) and the time-averaged A distribution (b) suggest that the system is approximately ergodic.

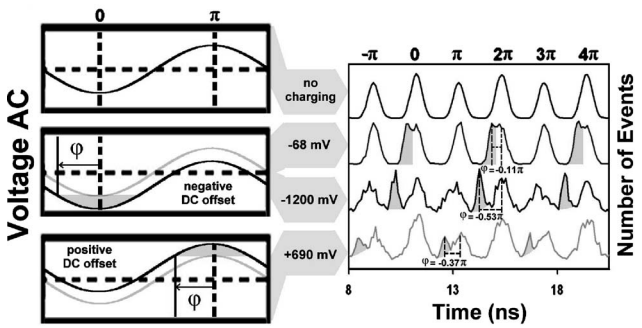

FIG. 7. Time-dependent voltage diagram and EL histograms of (top) typical cluster emission under ac excitation for comparison with cluster emission in the proposed presence of (middle) negative and (bottom) positive electrostatic charging of the injecting electrode. EL histogram bin width is approximately 97 ps.

The mechanism by which electrode-nanocluster coupling may change remains unknown and could involve dynamic changes in the molecule's orientation or position relative to the charge-injecting electrode, as well as small electromigration-induced electrode morphology changes. The three coupling regimes detailing the dynamics of typical, resonance-ac-excited electroluminescent clusters are sufficient for describing 100 of the 103 molecules for the duration of our experiments. In the remaining three molecules studied, however, EL arising from additional charge-transport mechanisms is observed. These three molecules further demonstrate the inherent heterogeneity of the break junction environment. The EL decay histograms of these clusters (Fig. 7, right) show additional light-emission peaks (shaded) phase-shifted from those appearing at π and 2π. This type of emission yields much narrower line shapes than

typical EL and may result from small dc offsets in the local potential due to electrostatic charging of islands near the nanocluster. Assuming a constant turn-on voltage for a particular cluster, the observed time shift in EL could arise from a voltage shift in the excitation potential such that the turn-on voltage is reached some time earlier. Static floating of a sinusoidal potential by even a few percent can cause an observable delay in the time at which the discrete cluster turn-on voltage is reached. The left panels in Fig. 7 illustrate how such an offset polarity and magnitude could translate into a phase shift, φ, in detection. In all the examples (Fig. 7, left), only portions of the sinusoidal potential exceeding the discrete cluster turn-on voltage (shading) may drive cathode or anode injection and EL. In the absence of charging (top panel), hole and electron injection proceed from the same electrode as the applied potential crosses the cluster turn-on voltage precisely at 0 or π. These conditions generate a "typical" EL decay trace with alternating anode and cathode peaks at 0 and π, respectively.

The proposed electrostatic charging of a nearby grain may perturb the local junction potential near an electroluminescent cluster by temporarily inducing a dc offset. Consistent with previous experiments, assuming that only the electron injection step occurs into a discrete energy level, negative offsets (middle panel) would result in earlier cluster turn-on from the anode, producing an additional EL peak detected slightly before the normal anode-injection EL peak (2π). Because negative offsets drive electron injection exclusively from the anode, any EL driven by a negative offset field should be detected in the range $(\pi, 2\pi)$. Conversely, positive offsets (bottom panel) might drive electron injection from the opposite polarity cathode, producing EL in the range $(0, \pi)$. Following this model, observed peak phase shifts away from their expected anode—or cathode-injection emission phases (times) of -0.11π, -0.53π, and -0.37π would correspond to dc offsets in the local potential of −68 mV, −1200 mV, and +690 mV, respectively. The observed emission switches back and forth between phase-shifted and non-phase-shifted EL, suggesting that the charging effect is not constant. Such transient charging of isolated grains could likely be modulated by electromigration and is consistent with the slow but dynamic electrode restructuring and dynamic coupling to individual nanoclusters observed in dc and ac experiments. In contrast to alternating anode- and cathode-injection peaks found in typical emission, the proposed additional charging-induced peaks appear only once per excitation period. This is presumably because the charging must be stable for at least several seconds, and raising the potential for injection from one electrode requires an equal lowering of the potential for injection from the opposite electrode one half period later.

IV. CONCLUSIONS

In summary, we have observed dynamic electrode-molecule couplings in electroluminescent gold break junctions. Phase locking the ac mode excitation and detection allows a phase-gated analysis of the photon stream and separation of the individual electrode contributions to charge transport in the absence and presence of static charging. These electroluminescent, molecular gold clusters within electromigrated gold break junctions are created *in situ* during the asymmetric writing process and act as nanoscale reporters of the electric field spanning the junction. The fluctuations in charge injection asymmetry are biased toward the anode, which is defined as the positive electrode during junction formation. This asymmetry is likely a general feature common to electromigrated gold break junctions arising from an inherently asymmetric fabrication process, and it is consistent with recently reported asymmetric Kondo resonances[30] and Coulomb blockades.[13] The optoelectronic properties of these systems arise from a combination of the electrical properties of the gold-insulator-gold junction with the optical properties of the isolated nanoclusters within the junction. Therefore, even at room temperature, the observable cluster emission reveals previously inaccessible information about the rich physics governing tunneling across the electromigrated gold break junctions so commonly employed in molecular electronics.

ACKNOWLEDGMENTS

J.I.G. acknowledges support from SREB and Mac-Arthur-Nunn programs, T.V. gratefully acknowledges support from the F.W.O. program, and R.M.D. appreciates support from The Dreyfus Foundation.

*Corresponding author.
Electronic address: dickson@chemistry.gatech.edu

[1] R. M. Metzger and M. P. Cava, in *Molecular Electronics: Science and Technology* (Blackwell Publishing, Inc., New York, 1998), Vol. 852, p. 95.
[2] M. A. Reed, C. Zhou, M. R. Deshpande, C. J. Muller, T. P. Burgin, L. Jones II, and J. M. Tour, Science **852**, 133 (1998).
[3] P. Avouris, Acc. Chem. Res. **35**, 1026 (2002).
[4] J. Park, A. N. Pasupathy, J. I. Goldsmith, C. Chang, Y. Yaish, J. R. Petta, M. Rinkoski, J. P. Sethna, H. D. Abruna, P. L. McEuen *et al.*, Nature (London) **417**, 722 (2002).
[5] W. Liang, M. P. Shores, M. Bockrath, J. R. Long, and H. Park, Nature (London) **417**, 725 (2002).
[6] H. Park, J. Park, A. K. L. Lim, E. H. Anderson, A. P. Alivisatos, and P. L. McEuen, Nature (London) **407**, 58 (2000).
[7] H. Park, A. K. L. Lim, A. P. Alivisatos, J. Park, and P. L. McEuen, Appl. Phys. Lett. **75**, 301 (1999).
[8] M. A. Reed, C. Zhou, C. J. Muller, T. P. Burgin, and J. M. Tour, Science **278**, 252 (1997).
[9] V. Mujica, M. Kemp, A. Roitberg, and M. Ratner, J. Chem. Phys. **104**, 7296 (1996).
[10] A. Nitzan and M. A. Ratner, Science **300**, 1384 (2003).
[11] J. B. Barner and S. T. Ruggiero, Phys. Rev. Lett. **59**, 807 (1987).
[12] C. S. Jiang, T. Nakayama, and M. Aono, Appl. Phys. Lett. **74**,

1716 (1999).
[13] R. Sordan, K. Balasubramanian, M. Burghard, and K. Kern, Appl. Phys. Lett. **87**, 013106 (2005).
[14] R. H. Fowler and L. Nordheim, Proc. R. Soc., London **119**, 173 (1928).
[15] R. C. Jaklevic and J. Lambe, Phys. Rev. Lett. **17**, 1139 (1966).
[16] A. N. Pasupathy, J. Park, C. Chang, A. V. Soldatov, S. Lebedkin, R. C. Bialczak, J. E. Grose, L. A. K. Donev, J. P. Sethna, D. C. Ralph *et al.*, Nano Lett. **5**, 203 (2005).
[17] Z. Yuan, B. E. Kardynal, R. M. Stevenson, A. J. Shields, C. J. Lobo, K. Cooper, N. S. Beattie, D. A. Ritchie, and M. Pepper, Science **295**, 102 (2002).
[18] M. S. Gudiksen, K. N. Maher, L. Ouyang, and H. Park, Nano Lett. **5**, 2257 (2005).
[19] H. J. Lee and W. Ho, Phys. Rev. B **61**, R16347 (2000).
[20] L. J. Lauhon and W. Ho, Science **451**, 219 (2000).
[21] N. Nilius, T. M. Wallis, and W. Ho, J. Chem. Phys. **117**, 10947 (2002).
[22] J. I. Gonzalez, T. H. Lee, M. D. Barnes, Y. Antoku, and R. M. Dickson, Phys. Rev. Lett. **93**, 147402 (2004).
[23] T. H. Lee, J. I. Gonzalez, J. Zheng, and R. M. Dickson, Acc. Chem. Res. **38**, 534 (2005).
[24] J. Lambe and R. C. Jaklevic, Phys. Rev. **165**, 821 (1968).
[25] J. Lambe and S. L. McCarthy, Phys. Rev. Lett. **37**, 923 (1976).
[26] S. L. McCarthy and J. Lambe, Appl. Phys. Lett. **30**, 427 (1977).
[27] T. H. Lee and R. M. Dickson, Proc. Natl. Acad. Sci. U.S.A. **100**, 3043 (2003).
[28] T. H. Lee and R. M. Dickson, J. Phys. Chem. B **107**, 7387 (2003).
[29] T.-H. Lee, J. I. Gonzalez, and R. M. Dickson, Proc. Natl. Acad. Sci. U.S.A. **99**, 10272 (2002).
[30] A. A. Houck, J. Labaziewicz, E. K. Chan, J. A. Folk, and I. L. Chuang, Nano Lett. **5**, 1685 (2005).
[31] J. Zheng, C. Zhang, and R. M. Dickson, Phys. Rev. Lett. **93**, 077402 (2004).
[32] M. Schimschak and J. Krug, Phys. Rev. Lett. **80**, 1674 (1998).
[33] L. H. Yu and D. Natelson, Nano Lett. **4**, 79 (2004).
[34] E. Irissou, M. C. Denis, M. Chaker, and D. Guay, Thin Solid Films **472**, 49 (2005).
[35] K. Juodkazis, J. Juodkazyte, V. Jasulaitiene, A. Lukinskas, and B. Sebeka, Electrochem. Commun. **2**, 503 (2000).
[36] Y. Xue, S. Datta, and M. A. Ratner, Chem. Phys. **281**, 151 (2002).
[37] T. Vosch, M. Cotlet, J. Hofkens, K. Van der Biest, M. Lor, K. Weston, P. Tinnefeld, M. Sauer, L. Latterini, K. Mullen *et al.*, J. Phys. Chem. A **107**, 6920 (2003).
[38] H. Yang and X. S. Xie, J. Chem. Phys. **117**, 10965 (2002).
[39] The average injection efficiency for one cluster was measured by exciting the EL with pulse pairs of opposite polarity at varying repetition rates. A $\sim \pm 1.5$ V ac field (measured into 50 Ω) produces approximately one photon for every 5000 excitation periods.